Computational Geosciences (2020) 24:807–818
https://doi.org/10.1007/s10596-019-9824-2

ORIGINAL PAPER

On the development of a relative permeability equation of state

Prakash Purswani[1] · Miral S. Tawfik[1] · Zuleima T. Karpyn[1] · Russell T. Johns[1]

Received: 14 September 2018 / Accepted: 7 May 2019 / Published online: 20 June 2019

Abstract

Standard compositional simulators use composition-dependent cubic equations of state (EoS), but saturation-dependent relative permeability and capillary pressure. This discrepancy causes discontinuities, increasing computational time and reducing accuracy. In addition, commonly used empirical correlations, such as the Corey relative permeability model, show a sole dependence of relative permeability on phase saturation, lumping the effect of other pore-scale phenomena into one tuning exponent. To rectify this problem, relative permeability has been recently defined as a state function, so that it becomes compositional dependent and single valued. Such a form of the relative permeability EoS can significantly improve the convergence in compositional simulation for both two- and three-phase flows. This paper revisits the recently developed EoS for relative permeability by defining relevant state variables and deriving functional forms of the partial derivatives in the state function. The state variables include phase saturation, phase connectivity, wettability index, capillary number, and pore topology. The developed EoS is constrained to key physical boundary conditions. The model coefficients are estimated through linear regression on data collected from a pore-scale simulation study that estimates relative permeability based on micro-CT image analysis. The results show that a simple quadratic expression with few calibration coefficients gives an excellent match to two-phase flow simulation measurements from the literature. The goodness of fit, represented by the coefficient of determination (R^2) value, is 0.97 for relative permeability at variable phase saturation and phase connectivity, and constant wettability, pore structure, and capillary number ($\sim 10^{-4}$). The quadratic response for relative permeability also shows excellent predictive capabilities.

Keywords Relative permeability · Phase connectivity · Equation of state · State function · Fluid flow in porous media · Two-phase flow

1 Introduction

Multiphase flow in porous media is of great interest in a wide array of applications including hydrocarbon recovery, groundwater resource utilization [1, 2], CO_2 storage [3], aquifer remediation [4, 5], and two-phase flow in proton-exchange membrane fuel cells [6, 7]. Each of these applications is governed by a multitude of underlying pore-scale phenomena, such as Haines jumps [8, 9], snap-offs [10, 11], corner flow [12], capillary and viscous fingering [2], diffusion and dispersion [13], dissolution/precipitation [14, 15], and wettability alteration [16–18].

Considering the breadth of multiphase-flow literature, studies can be classified into two categories: macroscopic and microscopic. In macroscopic studies, averaged transport properties, such as relative permeabilities and capillary pressure, are measured on core samples to capture the effect of these flow properties on macro-scale properties of interest, such as oil recovery. The averaged transport properties at the core scale act as a proxy to pore-scale processes, which govern the multiphase-flow process.

Standard compositional simulation employs the principles of continuum mechanics to model multiphase flow in complex porous media, using averaged transport properties. The most commonly used two-phase relative permeability model in commercial compositional simulators is the Corey model, which is an empirical correlation that assumes sole dependence of relative permeability on phase saturation. As explained in Khorsandi et al. [19], this has several limitations, including the necessity of phase labeling, which causes discontinuities as a phase disappears or changes to another phase, causing serious convergence and stability

✉ Prakash Purswani
pxp5185@psu.edu

[1] John and Willie Leone Family Department of Energy and Mineral Engineering, and the EMS Energy Institute, 110 Hosler Building, University Park, State College, PA 16802, USA

problems [19]. In addition, in order to include the effect of hysteresis, modification of the Corey model is used [20]. The modified model, however, assumes that phase saturation follows a particular path. Saturation history is not sufficient to consider the effect of phase distribution on multiphase flow [21]. Khorsandi et al. [22] proposed a new functional form for compositionally dependent relative permeability based on the state function concept that eliminates the need for phase labeling [22]. They demonstrated excellent predictive capability even for complex hysteretic flow. Khorsandi et al. [19] then proposed a new compositional simulation approach that eliminated the inconsistencies caused by saturation-based transport properties, demonstrating significant improvement compared to current commercial simulators, resolving stability and convergence issues, as well as increased robustness and accuracy [19].

With the advancement in X-ray micro-computed tomography (CT), the technology is utilized in several microscopic multiphase flow studies, allowing for visualization and quantification of previously theorized pore-scale processes [23–29]. Fast synchrotron-based X-ray tomography allows for real-time visualization of phenomena like cooperative pore filling, corner filling, droplet fragmentation, snap-off, and coalescence [23, 30, 31]. Avraam and Payatakes [30] were among the first to propose four main flow regimes observed during multiphase flow through porous media via 2D micromodel experiments. These included small and large ganglion dynamics, drop traffic flow, and connected pathway flow. It was observed that as the flow rate of the wetting phase increased, the flow regime shifted from large ganglion dynamics to small ganglion dynamics to drop traffic flow to connected pathway flow. A simultaneous increase in relative permeabilities was observed [30]. These findings have been recently corroborated through experiments and simulation studies by Armstrong and coworkers [31, 32].

In more recent studies by Pak et al. [29] and Khishvand et al. [33], the authors conducted micro-CT experiments to visualize and quantify the trapped non-wetting phase structures at variable capillary numbers. In addition, it was observed during drainage cycles that at higher flow rates, the number of individual non-wetting phase clusters increases. The authors also noted the importance of the pore structure by observing that droplet fragmentation was not severe in homogenous rocks like sandstones compared to the more complex carbonate pore structures [29]. In such studies, researchers have adopted various quantitative approaches for characterizing phase connectivity, including Euler characteristic, coordination number, percolation threshold, fractal dimension [34], and specific fluid-fluid and fluid-solid interfacial areas [27, 35].

There is enough evidence in the literature that suggests that multiphase flow in porous media is affected by rock properties: rock mineralogy, surface roughness, pore geometry, pore topology, and heterogeneity; fluid properties: viscosity and density; and rock-fluid and fluid-fluid interactions: wettability, adsorption, precipitation, chemical dissolution, and interfacial tension [34]. Avraam and Payatakes [36], recognized the importance of the dependence of relative permeability on various parameters, in addition to fluid saturation, such as capillary number, viscosity ratio between injected and displaced fluid, bond number, advancing and receding contact angles, coalescence factor, pore geometrical and topological factor, and the history of flow. Within reason, a number of these parameters were varied to evaluate their impact on fluid distribution and relative permeabilities [36].

Khorsandi et al. [22] proposed an equation-of-state (EoS) approach for modeling relative permeabilities as a state function. The main advantage of this approach is that it is physically based and ensures a single valued solution for relative permeability. The contributing parameters that affect relative permeabilities were saturation of the fluid phases, phase connectivity, capillary number, wettability of the medium, and the pore structure of the medium. The authors evaluated the importance of phase saturation and connectivity on relative permeabilities and found a good match against experimentally published data [22]. However, there was no discussion about the verification of the EoS being a valid state function nor its validity at limiting boundaries of the state variables.

In this research, we present a structured workflow for the development of an equation of state (EoS) for relative permeability using a response surface modeling approach. We define relevant boundary conditions to physically constrain the EoS under limiting conditions and derive functional forms for the partial derivatives. For this development, we implement similar state variables proposed by Khorsandi et al. [22]. The calibrating parameters in the final form of the EoS are determined through linear regression on the data presented in the recent literature that presents measurements of phase saturation, phase connectivity, and relative permeabilities. In the following sections, we outline the development of the model, provide the description of the boundary conditions, and present the results that show the fit of the model to the literature data.

2 Methodology

2.1 Development of a state function

A state function, by definition, is a property whose value depends only on the condition or state of the system irrespective of the path taken to reach that state [37, 38].

This implies that for relative permeability to be a state function, it must only have one value at a given set of the variables considered. To satisfy this condition, the developed relative permeability function must be an exact differential. For an exact differential, the partial derivative coefficients must satisfy the Euler reciprocity relation [39]. In thermodynamics, for a property that is a function of n variables to be an exact differential, it must satisfy N_E reciprocity relations, where N_E is the number of conditions given by

$$N_E = \sum_{i=1}^{n-1} i. \tag{1}$$

For a state function $dQ = f_1 dx_1 + f_2 dx_2 \ldots + f_n dx_n$, the conditions will be of the form

$$\left.\frac{\partial f_i}{\partial x_j}\right|_{x_k, k\neq j} = \left.\frac{\partial f_j}{\partial x_i}\right|_{x_k, k\neq i}, \text{for } \mathbf{i}\ \forall[1:n-1];\ \mathbf{j}\ \forall[i+1:n];\ \mathbf{k}\ \forall[1:n]. \tag{2}$$

Another condition contributing to the validity of a state function is whether the state variables considered are independent. Properties are considered independent of each other when one property can be varied while all other input properties are held constant. On analyzing microscopic multiphase flow experimental studies in the literature, it is observed that saturation and phase connectivity are independent variables except when saturation is exactly one (e.g., [40]). At the same saturation value, multiple fluid configurations can exist leading to widely different phase connectivity.

As discussed previously, there are numerous pore-scale variables that may contribute to changes in relative permeability. Hence, given the complex nature of the problem, there are many degrees of freedom that can be specified to fully define relative permeability as an EoS. Including all the parameters that contribute to changes in transport properties in the state function would theoretically result in an exact match of the literature data. Practically, however, a very complex model would be required to account for all state variables that affect relative permeability. Therefore, in this research, we use the minimum number of variables that sufficiently define the state of the system, exhibiting a good match with literature data, and allowing for reliable relative permeability predictions, with an acceptable degree of accuracy.

Khorsandi et al. [22] proposed an equation-of-state approach (Eqs. 3 and 4) to calculate the change in relative permeability as a function of five measurable, pore-scale state variables [22].

$$k_{r_j} = f\left(S_j, \hat{\chi}_j, I_j, N_{\text{ca}}, \lambda\right). \tag{3}$$

Expressing Eq. 3 in exact differential form,

$$dk_{r_j} = \frac{\partial k_{r_j}}{\partial S_j} dS_j + \frac{\partial k_{r_j}}{\partial \hat{\chi}_j} d\hat{\chi}_j + \frac{\partial k_{r_j}}{\partial I_j} dI_j + \frac{\partial k_{r_j}}{\partial N_{\text{ca}}} dN_{\text{ca}} + \frac{\partial k_{r_j}}{\partial \lambda} d\lambda. \tag{4}$$

where S_j represents saturation of phase j, $\hat{\chi}_j$ represents connectivity in terms of the normalized Euler characteristic of phase j, I_j is the wettability index of phase j, N_{ca} is the capillary number and λ is the pore structure.

At constant wettability ($dI_j = 0$), constant pore structure ($d\lambda = 0$), and constant flow rate and fluid properties (i.e., $dN_{\text{ca}} = 0$), Eq. 4 reduces to Eq. 5.

$$dk_{r_j} = \left(\frac{\partial k_{r_j}}{\partial S_j}\right)_{\hat{\chi}_j} dS_j + \left(\frac{\partial k_{r_j}}{\partial \hat{\chi}_j}\right)_{S_j} d\hat{\chi}_j. \tag{5}$$

For the simplified relative permeability state function defined in Eq. 5, only one reciprocity condition (see Eq. 1) must be honored as shown by Eq. 6.

$$\frac{\partial}{\partial \hat{\chi}_j}\left(\frac{\partial k_{r_j}}{\partial S_j}\right)_{\hat{\chi}_j} = \frac{\partial}{\partial S_j}\left(\frac{\partial k_{r_j}}{\partial \hat{\chi}_j}\right)_{S_j}. \tag{6}$$

By forcing relative permeability to satisfy Eq. 5, we ensure that there is only one value of relative permeability as a function of two variables, while simultaneously capturing the essential physics. The error introduced by this approach is minimized by tuning to literature data.

2.2 Phase connectivity

Finding a unique mathematical definition for connectivity in porous media has been an active point of research [41]. A number of connectivity parameters have been discussed in the literature such as the Euler characteristic [42], percolation threshold [43], connectivity function [44], contour tree connectivity [41], coordination number, and fractal dimension [34]. Out of these measures, the Euler characteristic (χ) has been the simplest and most widely used measure of connectivity in porous media [44, 45].

The Euler characteristic is a topological invariant originally proposed by Leonhard Euler for a polyhedron as the alternating sum of vertices (V), edges (E), faces (F), and objects (O) as shown in Eq. 7 [46]. Extending the concept to more complex structures, the Euler Poincaré formula (Eq. 8) has been widely used for quantifying connectivity of microstructures. The Euler characteristic values range from $-\infty$ to $+\infty$ where a highly connected phase has a large negative value and a highly disconnected phase has a large positive value.

$$\chi = V - E + F - O. \tag{7}$$

$$\chi = \beta_0 - \beta_1 + \beta_2. \tag{8}$$

The parameters β_0, β_1, andβ_2 are the zeroth, first, and second Betti numbers, respectively. β_0 represents the number of clusters, β_1 is the number of holes or redundant loops (the maximum number of breaks that can be made without having the cluster split into two as explained by Herring et al. [47], and β_2 is the number of enclosed voids.

The Euler characteristic depends on saturation, saturation history, pore topology, and the scale of the measurement. To allow for better comparison based on phase connectivity only, we must normalize the Euler characteristic to eliminate such effects. Herring et al. developed a normalization scheme that eliminated the effect of pore structure by dividing $\chi_{\text{non-wetting phase}}$ by $\chi_{\text{pore structure}}$, which is equivalent to the Euler characteristic at 100% phase saturation [47]. However, this only sets an upper bound to the value of the normalized Euler characteristic, $\hat{\chi}$, where $-\infty < \hat{\chi} < 1$. Khorsandi et al. [22] modified this normalization scheme to eliminate the effect of measurement scale and phase saturation, as well as to set a lower bound to the value of $\hat{\chi}$ [22]. In this paper, we use a simpler expression for the normalization of the Euler characteristic (Eq. 9) such that $\hat{\chi}$ is bounded between 0 and 1.

$$\hat{\chi}_j = \frac{\chi_j - \chi_{\max}}{\chi_{\min} - \chi_{\max}}, \tag{9}$$

where $\chi_{\max}$ represents the limiting case for a completely dispersed phase which is expected to occur when *all* the pores in the porous medium are filled with the phase but *no* throats are filled to connect the pores and $\chi_{\min}$ represents the case where a phase is fully connected, occupying 100% of the pore space. $\chi_{\min}$ can be easily estimated as the Euler number of the pore space from its micro-CT image, whereas $\chi_{\max}$ can be estimated as the number of pores from the extracted pore network of the pore space, or from the coordination number of the rock type and its $\chi_{\min}$ value. These minimum and maximum values of the Euler characteristic are independent of the fluid type.

Equation 9 defines an intrinsic connectivity parameter for a homogeneous medium that is no longer dependent on the pore volume considered. A value of zero for the dimensionless phase connectivity means the phase is disconnected completely, while a value of one is perfect connectivity.

2.3 Development of relative permeability EoS

For the development, the EoS (i) must satisfy the reciprocity relation shown in Eq. 6, (ii) must honor physical boundary conditions, and (iii) must be the simplest functional form possible to minimize overfitting of test data. Therefore, we consider that the relative permeability state function takes a simple form, such that the partial differential coefficients are linear in $\hat{\chi}_j$ and S_j. Thus, we make the relative permeability state function a quadratic response to S_j and $\hat{\chi}_j$ expressed by Eq. 10.

$$k_{r_j} = \alpha_0 + \alpha_1 \hat{\chi}_j + \alpha_2 S_j + \alpha_{11} \hat{\chi}_j^2 + \alpha_{22} S_j^2 + \alpha_{12} \hat{\chi}_j S_j. \tag{10}$$

Next, we describe the principle limiting conditions presented in Table 1 to constrain the EoS. The first constraint is that for both saturation and phase connectivity equal to 1.0, the relative permeability must be 1.0. At phase saturation just below 1.0, the phase connectivity can theoretically vary over its entire range, although physically only a small range is likely for a given set of variables.

We set the phase connectivity to be 1.0 and saturation to be 0.0 for the second constraint. At low phase saturation, in general, the phase connectivity should be low; however, for a wetting phase under extreme wetting conditions, the connectivity could be high as well. Also, for a non-wetting phase (say oil), the region near $\hat{\chi}_j = 0$ and $S_j = 0$ is a plausible physical region for cases such as film drainage when two other phases are present (say gas and water). Otherwise, it is unlikely to achieve flow near this region.

The third and fourth constraints are set to ensure that the partial derivatives are positive over the entire $\hat{\chi}_j$ and S_j space. These constraints could be removed if more experimental data is available to improve the values of relative permeability in regions near these limits. We found it necessary to include these constraints for the data examined in this paper.

We did not constrain the relative permeability function at $S_j = 1$ and $\hat{\chi}_j = 0$, as it is not physical to reach this value of connectivity. That is, at exactly a saturation of 1.0, the phase connectivity must be 1.0 in that it is no longer independent, but at a saturation of 0.99 and $\hat{\chi}_j = 0$, the relative permeability should be zero. We omitted this constraint from the fitting procedure based on the recognition that complex porous media would likely never have values near this region. It is likely that there is a limiting value of $\hat{\chi}_j$ as a function of saturation based on pore morphology and other state variables.

Upon implementing these physical constraints, we obtained the final form of the model shown below.

$$k_{r_j} = \alpha_{11}\left(1 - 2\hat{\chi}_j + \hat{\chi}_j^2\right) + \alpha_{22}\left(-2S_j + S_j^2 + \hat{\chi}_j S_j\right) + \hat{\chi}_j S_j. \tag{11}$$

The coefficients α_{11} and α_{22} are determined through linear regression on measured data. Evaluation of the partial derivatives of Eq. 11 gives

$$\left(\frac{\partial k_{r_j}}{\partial \hat{\chi}_j}\right)_{S_j} = 2\alpha_{11}\hat{\chi}_j + S_j(1 + \alpha_{22}) - 2\alpha_{11}, \tag{12}$$

$$\left(\frac{\partial k_{r_j}}{\partial S_j}\right)_{\hat{\chi}_j} = \hat{\chi}_j(1 + \alpha_{22}) + 2\alpha_{22}S_j - 2\alpha_{22}. \tag{13}$$

Table 1 Physical constraints imposed on the relative permeability response by considering 683 key limiting conditions that affect relative permeability as a function of phase saturation and 684 phase connectivity

Physical constraint	Remarks
$k_{rj} = 1$ at $S_j = 1$ and $\hat{\chi}_j = 1$	Relative permeability at 100% saturation must be 1
$k_{rj} = 1$ at $S_j = 0$ and $\hat{\chi}_j = 1$	Relative permeability with low phase saturation should be negligible
$\frac{\partial k_{rj}}{\partial \hat{\chi}_j}\Big\vert_{S_j=0} = 0$ at $\hat{\chi}_j = 1$	The change in relative permeability with full phase connectivity should be negligible near full phase connectivity
$\frac{\partial k_{rj}}{\partial S_j}\Big\vert_{\hat{\chi}_j=0} = 0$ at $S_j = 1$	The change in relative permeability with full phase saturation should be negligible near 100% saturation

The phase is assumed nonwetting, although extensions to other phases are easily possible

Euler reciprocity shows that these derivatives define a state function (Eq. 6). That is,

$$\frac{\partial}{\partial \hat{\chi}_j}\left(\frac{\partial k_{r_j}}{\partial S_j}\right)_{\hat{\chi}_j} = \frac{\partial}{\partial S_j}\left(\frac{\partial k_{r_j}}{\partial \hat{\chi}_j}\right)_{S_j} = 1 + \alpha_{22}. \tag{14}$$

The exact differential form (Eq. 5) then becomes from Eqs. 12 and 13,

$$dk_{r_j} = \left[2\alpha_{11}\hat{\chi}_j + S_j(1+\alpha_{22}) - 2_{\alpha_{11}}\right] d\hat{\chi}_j + \left[\hat{\chi}_j(1+\alpha_{22}) + 2_{\alpha_{22}} S_j - 2_{\alpha_{22}}\right] dS_j. \tag{15}$$

2.4 Comparison to the development in Khorsandi et al. [22]

The relative permeability EoS proposed by Khorsandi et al. is shown in Eq. 16 [22]

$$k_{r_j} = C_k \left(\phi_j - \phi_{r_j}\right)^{n_k}, \tag{16}$$

where ϕ_j is the phase distribution term defined as $S_j + \alpha_\varphi \chi_j$; ϕ_{r_j} is the residual phase distribution of phase j; and C_k, α_φ, and n_k are tuning parameters. It was assumed in this formulation that the ratio of the two partial differential coefficients was constant. The form of Eq. 16 allowed for direct use of the Corey model, while also making the equation simple. Although Eq. 16 satisfies reciprocity, it does not satisfy all boundary conditions in Table 1 and likely is not reliable except near the tuned experimental data.

We set the value of n_k to 2 in Eq. 16 to get Eq. 17.

$$k_{r_j} = C_k \left(S_j^2 + \alpha_\varphi^2 \chi_j^2 + \phi_{r_j}^2 + 2\alpha_\varphi S_j \chi_j - 2S_j \phi_{r_j} - 2\chi_j \phi_{r_j}\right). \tag{17}$$

Comparing our development in Eq. 11 to Eq. 17, we see

$$C_k = \alpha_{22}, \tag{18}$$

$$\alpha_\varphi = \pm\sqrt{\frac{\alpha_{11}}{\alpha_{22}}}, \tag{19}$$

$$\phi_{r_j} = \pm\sqrt{\frac{\alpha_{11}}{\alpha_{22}}}. \tag{20}$$

More complicated cubic or higher-order polynomial equations could also be used, but the simplest form that reasonably matches experimental data and boundary conditions is preferred to avoid over-fitting. Most importantly, the EoS developed in this paper honors the physical boundary constraints presented in Table 1. The response surface formulation provides justification for Eq. 16, although future research could define a form of Eq. 16 that honors physical constraints like those in Table 1.

In Fig. 1, we illustrate that once the EoS is determined, the real path from the initial to the final state can be separated into a constant saturation path followed by a constant phase connectivity path or vice versa to arrive at the same final state. In this way, relative permeability can be calculated by integrating the individual partial differential coefficients to arrive at the final state's relative permeability. The shortcoming of such an approach is that it requires phase connectivity values at the initial and the final state, which is not readily available unless sophisticated techniques such as X-ray micro-CT are implemented. One way of overcoming this shortcoming is to determine a functionality between phase connectivity and phase saturation so as to bypass the dependence of relative permeability on phase connectivity. This provides an avenue for future research. Khorsandi et al. [22] solved this problem by assuming that the change in connectivity with saturation is constant for any drainage path, and similarly for any imbibition path. They used simple but different models for drainage and imbibition and tuned them to available data. From these fixed tuned models, they could predict hysteretic scans that began at different saturations.

2.5 Estimation of the coefficients of the EoS

The data set used for estimating the coefficients of the model in Eq. 11 is from Armstrong et al. [31]. In their paper, the authors coupled experimental research with simulations to study the effect of phase topology on macroscopic system behavior during two-phase flow in a porous medium. Micro-flow experiments were conducted in a sintered glass sample with chemically doped water as the

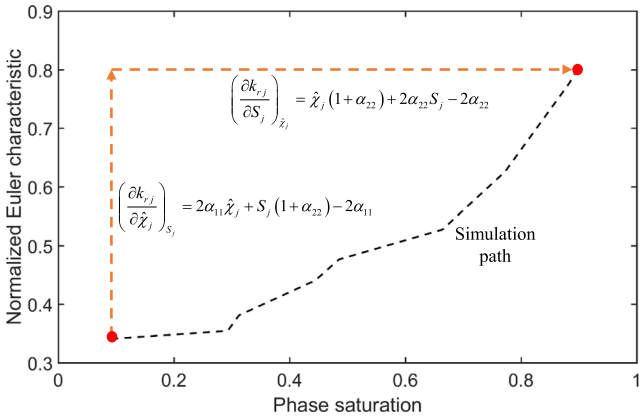

Fig. 1 Illustration showing the EoS state approach on a real path (simulation) taken during two-phase flow simulation in S_j and $\hat{\chi}_j$ space

wetting phase and decane as the non-wetting phase. The two phases were co-injected at different fractions maintaining steady-state conditions, and three different flow rates were tested to represent three different capillary numbers, namely 10^{-4}, 10^{-5}, and 10^{-6}. From the segmented images acquired during micro-flow experiments, 11 different fluid configurations (each representing a different fluid saturation arrangement) were used as the initial condition for two-phase flow simulations to determine relative permeabilities for a wider range of capillary numbers obtained by varying fluid properties during these simulations. A 4D connected component algorithm was implemented to track the fluid ganglion during simulations for estimating phase connectivity.

The full data set is displayed in Fig. 2. Figure 2a shows the data for phase relative permeability while Fig. 2b shows the data for phase connectivity, which is measured as a normalized Euler characteristic using Eq. 9. The phase shown here is the non-wetting phase because the Euler characteristic for the wetting phase was not reported.

Table 2 Euler characteristic values estimated through 2D extrapolation for the pore structure 689 used during simulations in Armstrong et al. [31]

$\chi_{\max}$	5788
$\chi_{\min}$	−10, 704

To calculate the normalized Euler characteristic values, $\hat{\chi}_j$, $\chi_{\max}$, and $\chi_{\min}$ need to be known. Because the number of pores and the Euler number of the pore structure were not reported, a 2D extrapolation was carried out on the data for $N_{\text{ca}} = 1$, which showed the maximum and minimum values for the Euler number. Large capillary numbers imply very low interfacial tension, which may explain the largest and smallest connectivity values observed.

We assumed a planar relationship among k_{r_j}, S_j, and $\hat{\chi}_j$ for the 2D extrapolation

$$k_{r_j} = AS_j + B\hat{\chi}_j + C. \tag{21}$$

Three-point extrapolation was carried out such that the extrapolated values were near the actual data as opposed to extrapolation on the entire data, which could lead to errors in estimation. The first three data points of the Euler number were used for determining $\chi_{\max}$, where k_{r_j} was set to 0, while the last three data points were used for determining $\chi_{\min}$, where k_{r_j} was set as 1. Simultaneously, the same three data points on either end were used for fitting lines through S_j and $\hat{\chi}_j$ for fixed N_{ca}, which were then intersected with the plane (Eq. 21) to estimate $\chi_{\max}$ and $\chi_{\min}$ values. The extrapolated values for the Euler characteristic of the pore structure are shown in Table 2.

3 Results and discussion

In this section, we present the results for the fitted quadratic response for relative permeability. The sub-data set of

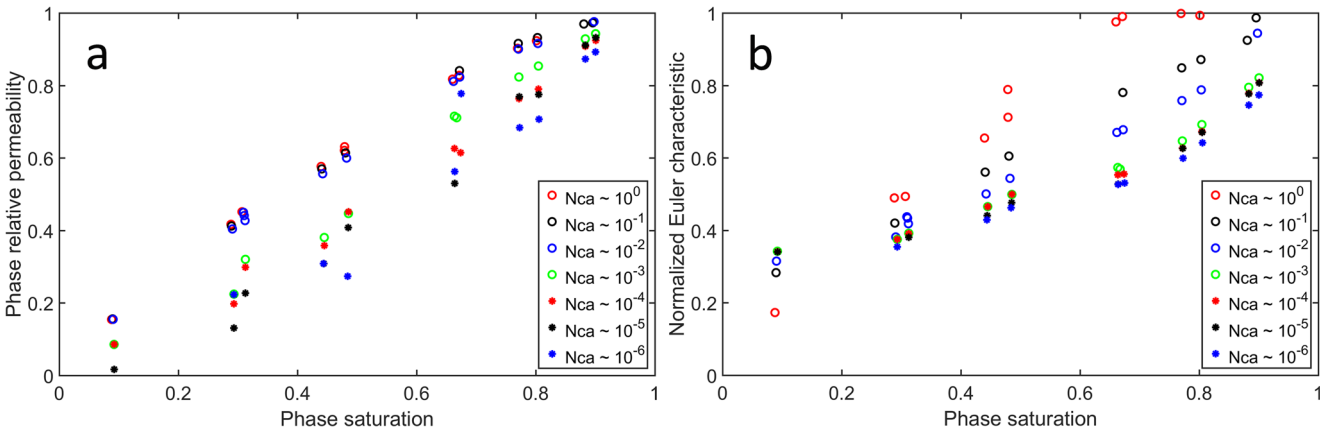

Fig. 2 Phase saturation, relative permeability, and normalized Euler connectivity for different capillary numbers used for fitting the quadratic response for relative permeability as well as for prediction purposes. Courtesy Dr. Ryan T. Armstrong. Data from Armstrong et al. [31]

Table 3 Model coefficients and the goodness of quadratic response surface fit to phase saturation and phase connectivity to the data presented in Armstrong et al. [31] at the N_{ca} of $\sim 10^{-4}$

α_{11}	−0.229
α_{22}	−0.589
R^2	0.971
Root mean squared error	0.147

capillary number $\sim 10^{-4}$ was used for response surface fitting. This fit was used to predict data sets at different capillary numbers. The goodness of fit is evaluated using residual error and R^2 values. Further, we present the partial derivative coefficient to the exact differential of relative permeability as a function of phase saturation and phase connectivity. Finally, we compare response surfaces generated for different capillary numbers using linear regression on the individual sub-data sets to evaluate the impact of the capillary number.

3.1 Quadratic response for relative permeability

We used linear regression with Matlab® to find the coefficients in the proposed model described in Eq. 11 that best fits the data set at the fixed capillary number of $\sim 10^{-4}$. Table 3 provides the information for the fitting parameters and the goodness measure of the fit.

The contour map of the response surface fit is shown in Fig. 4. The dots represent the data points at the fixed capillary number of $\sim 10^{-4}$ used for estimating the coefficients for the response surface. The corresponding plot for the residual error is shown in Fig. 3. As shown, the quadratic response gives small residual error values scattered around 0 with a mean of −0.009, showing little systematic error.

As shown in Fig. 4, the general trends of relative permeability versus saturation and relative permeability versus phase connectivity are honored, where relative permeability increases as saturation and phase connectivity increase. The contour map gives the relative permeability value for a known value of normalized phase connectivity and its corresponding value of phase saturation, irrespective of the path/direction a particular experiment/simulation may take. The contour map is also independent of the phase label (gas, oil, or water, for example). This is valid for the fixed wettability, pore structure, and capillary number used in the development of this quadratic response.

We present a notional boundary on the contour plot in Fig. 4, which represents the limits of possible physical experimental/simulation conditions. The regions below and to the right of the curve are extreme cases controlled by the topology of the rock structure itself, as well as other variables such as wettability. This region suggests that even at a very high phase saturation, the phase remains extremely disconnected. Such a case would be highly unusual to occur, especially in real porous media. It may occur in theoretical porous media with a highly disconnected pore structure or a pore structure with a very large aspect ratio between the pore and connecting throats so that very high capillary forces are required for the phase to pass through. Since there is insufficient data in this region, the prediction from our quadratic response fit may not lead to conclusive results for this region. A similar "unrealistic" region could be present in the upper left corner of the contour map, although this is not shown in Fig. 4. To achieve low saturations with high connectivity would require very thin wetting films or spreading of an intermediate wetting phase (in three-phase systems), where even at very low phase saturation a phase remains highly connected. Although the phase would remain highly connected, the relative permeability would be small in this region of S_j and $\hat{\chi}_j$ space owing to small saturation. More experimental studies should be conducted under extreme conditions and varying wetting states and pore topology of the medium to acquire more complete data sets to enhance predictive capabilities of these cases and to capture the loci of zero relative permeabilities in S_j and $\hat{\chi}_j$ space.

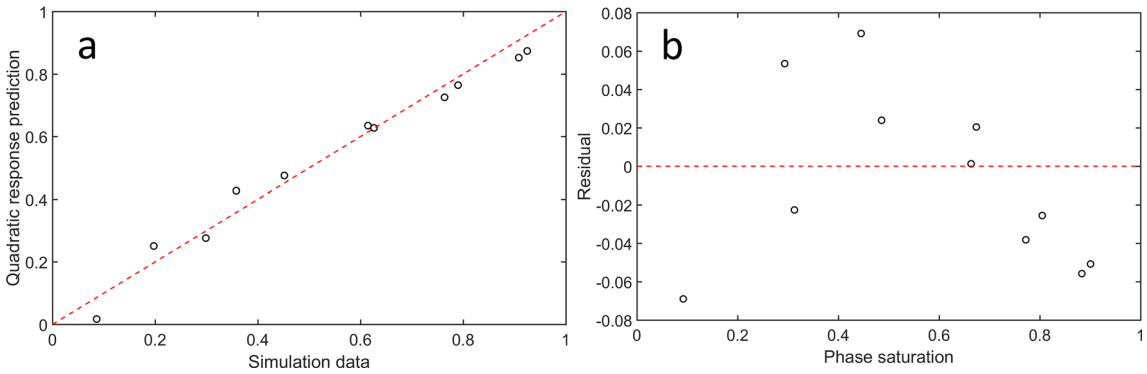

Fig. 3 **a** Quadratic response prediction versus simulation data. **b** Residual between the predicted and simulation measurements for relative permeability based on the response surface fit (Fig. 4)

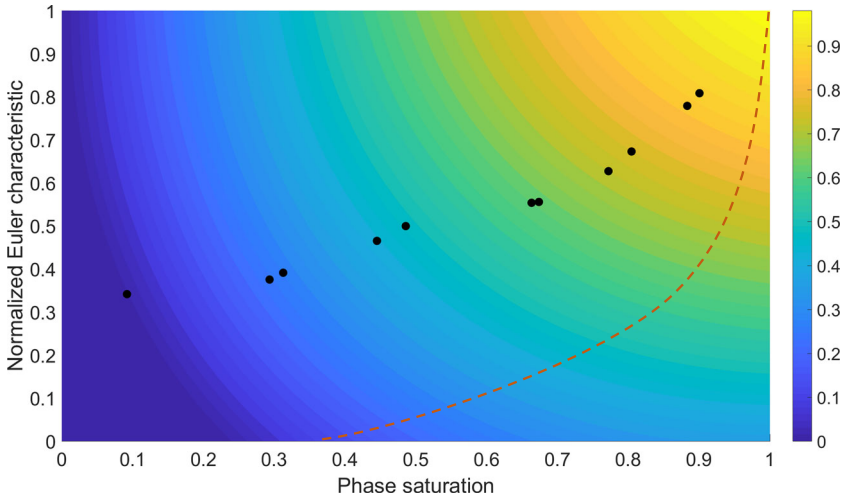

Fig. 4 Contour map of the response surface of relative permeability as a function of phase saturation and normalized Euler connectivity. The capillary number ($\sim 10^{-4}$), wettability, and pore structure have been kept constant. Data points shown as black dots were taken from the two-phase flow simulations presented in Armstrong et al. [31]. The dashed line represents a limiting boundary of plausible values

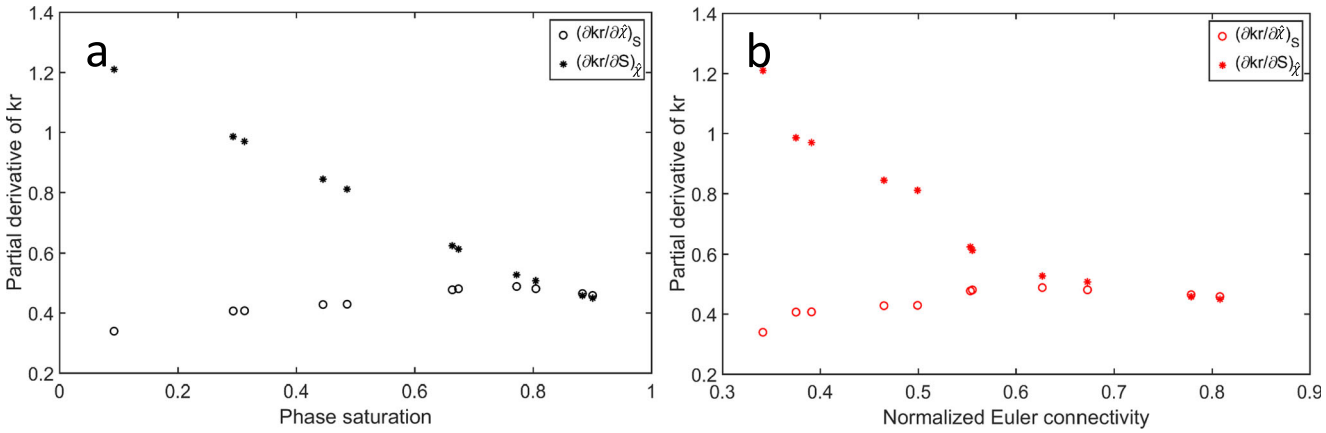

Fig. 5 Partial derivative coefficients (calculated using Eqs. 12 and 13) expressed as a function of **a** phase saturation and **b** normalized Euler connectivity

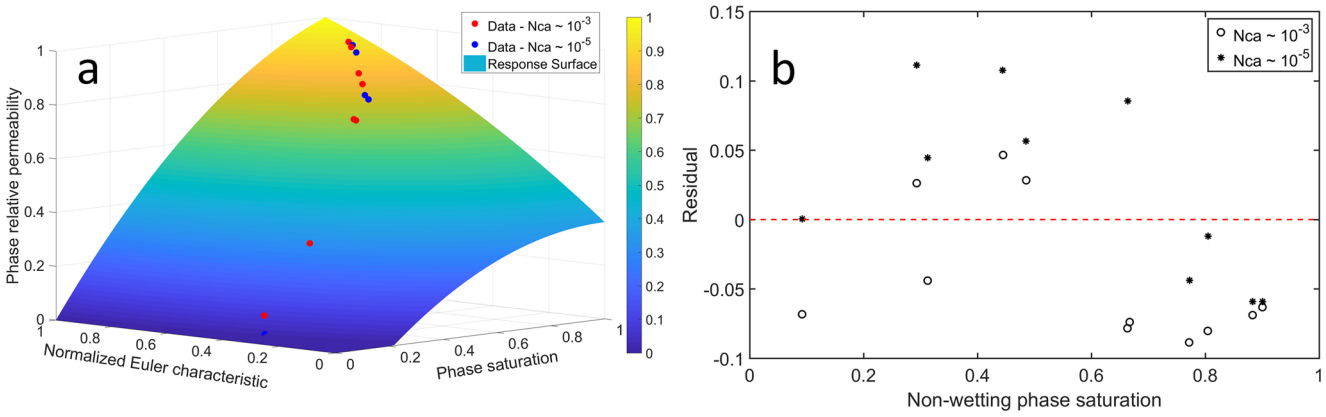

Fig. 6 **a** Prediction of relative permeability and **b** residual error for capillary numbers $\sim 10^{-3}$ and $\sim 10^{-5}$ based on the response surface fit to capillary number 10^{-4} described in Fig. 4

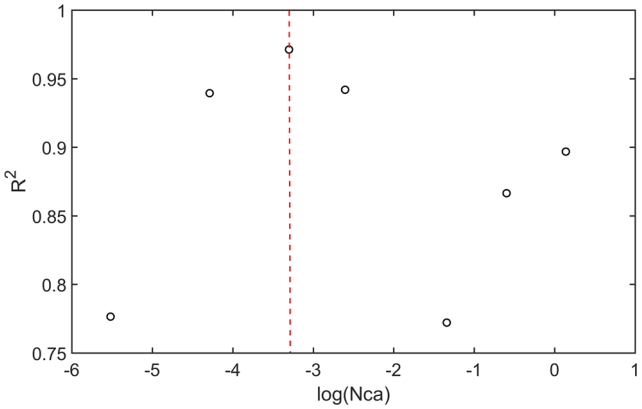

Fig. 7 R^2 error for prediction of data at different capillary numbers using the sub-data set at a capillary number of $\sim 10^{-4}$ as the fitted response surface

In Fig. 5, the partial differential coefficients expressed in the final form of the exact differential (Eq. 15) are shown as a function of phase saturation (Fig. 5a) and phase connectivity (Fig. 5b). Both partial derivatives w.r.t. relative permeability are always positive, suggesting that relative permeability increases with an increase in S_j as well as $\hat{\chi}_j$. We further observe that the rate of increase in relative permeability decreases with increasing saturation, whereas the rate of increase of the relative permeability with increasing phase connectivity increases, although this increase is minor and plateaus near $\hat{\chi}_j$~0.55. This suggests that the effect of an increase in phase saturation on relative permeability slowly declines, while the effect of phase connectivity grows. This is consistent with our understanding that for a phase to be sufficiently connected in the porous medium, some phase saturation should exist.

3.2 Quadratic response prediction at neighboring conditions

We now present the predictive capability of the fitted response surface to neighboring conditions. We use the same data set by Armstrong et al. [31] but at capillary numbers of $\sim 10^{-3}$ and $\sim 10^{-5}$. This ensures that the pore structure and wetting conditions remain the same between the fitted and the predicted cases. The plots for the response and the corresponding residual errors are shown in Fig. 6.

Figure 6 shows that the predicted response fits the data well. The residual errors between the predicted and actual relative permeability values show little systematic errors and R^2 values near $\sim$ 0.94 for both capillary numbers. It is likely that the capillary number impacts these values, as is discussed in the next section in more detail.

3.3 Effect of capillary number

To capture the effect of the capillary number on relative permeability, we use the surface fits to predict relative permeability at different capillary numbers ranging from $\sim 10^0$ to $\sim 10^6$. The goodness measure of these prediction cases is shown in Fig. 7.

From Fig. 7, we see that the R^2 value showing the goodness of fit is the maximum for capillary number $\sim 10^{-4}$ marked by the dashed red line. This is because the regression was carried out using this capillary number sub-data set. As stated earlier, the R^2 values in the neighborhood of the fitted response are excellent at about 0.94; however, as we move two to three orders of magnitude away from the original capillary number, the prediction with N_{ca} $\sim 10^{-4}$ leads to erroneous values. This clearly suggests the importance of the capillary number as a parameter that affects relative permeability. This is also shown in Fig. 8 for the fitted quadratic responses to individual sub-data sets at different capillary numbers (see Table 4 for fitting parameters). As the capillary number increases, the response surface becomes more planar, showing that the dependence of relative permeability on phase connectivity is reduced significantly while relative permeability becomes more sensitive to the change in saturation. The occurrence

Fig. 8 Quadratic response surface fits to sub-data sets at different capillary numbers

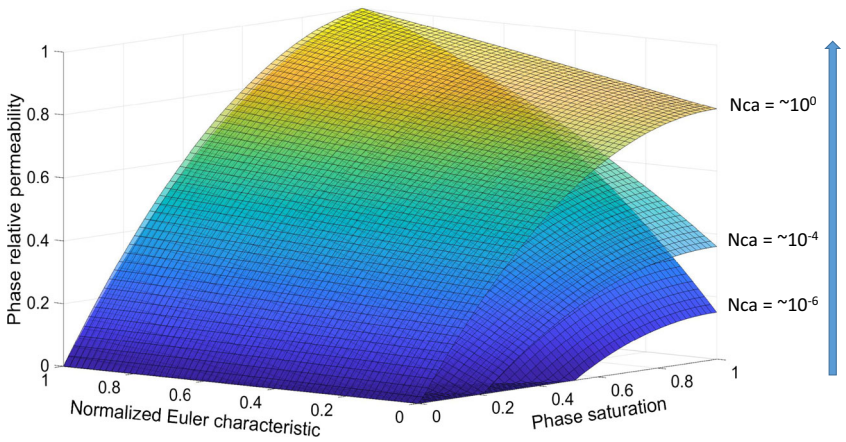

Table 4 Coefficients for the quadratic response and goodness measures for the quadratic response surface fits to sub-data sets at different capillary numbers shown in Fig. 8

Coefficients for the quadratic response and goodness measure	Capillary number		
	$\sim 10^0$	$\sim 10^{-4}$	$\sim 10^{-6}$
α_{11}	−0.009	−0.229	−0.517
α_{22}	−0.806	−0.589	−0.667
R^2	0.994	0.971	0.863
Root mean squared error	0.064	0.147	0.249

of these observations can be quantitatively observed in Table 4, where the magnitude of the α_{11} term decreases significantly at a higher capillary number. A sharp decrease in the magnitude of this term explains the reduced effect of phase connectivity (see Eq. 11). Overall, these observations are consistent with those observed by Armstrong et al. [31], where connectivity was found to be larger at greater capillary numbers and therefore relative permeability becomes more strongly dependent on phase saturation [31].

In Fig. 9, we show typical Corey fit to the data at extreme capillary numbers. The fit to the exponent was <1 for the high capillary number case and >1 for the low capillary number case. These exponents govern the curvature of the relative permeability change with respect to saturation, which causes a slower or faster increase in relative permeability as saturation changes. These plots reveal the inherent importance of phase connectivity implicitly assumed in Corey's approach for fitting relative permeability. The slower/faster change in relative permeability as seen in Fig. 9 is the result of the changes in phase connectivity. Such relative permeability curves are also observed during microemulsion/excess oil and microemulsion/excess brine relative permeability measurements conducted by Delshad et al. where the microemulsion phase relative permeability was observed to increase sharply [48]. This increase was attributed to the wettability and low interfacial tension of the microemulsion phase, which in principle improved connectivity to increase relative permeability.

4 Conclusions

In this paper, we present the development of a physically based quadratic state function for relative permeability in phase saturation and phase connectivity. The coefficients of the EoS are determined through linear regression on two-phase flow simulation data from the literature. The following conclusions can be drawn under the assumptions in which this study is conducted.

- A simple quadratic response for relative permeability gives an excellent fit to simulation data at fixed capillary numbers.
- The quadratic response fit acquired from one data set shows excellent predictive capabilities at similar flow conditions. However, away from original conditions, the predictive capability of the kr response surface decreases owing to the dependence on the capillary number.
- Connectivity increases faster at low saturations than at high saturations for large capillary numbers. This explains the small Corey exponents obtained in laboratory cores for ultra-low interfacial tension experiments. The reverse is true for a small capillary number where capillary effects dominate.

Although the model presented in this paper may not be the only solution, our approach was designed to seek the simplest EoS that honors key limiting physical constraints

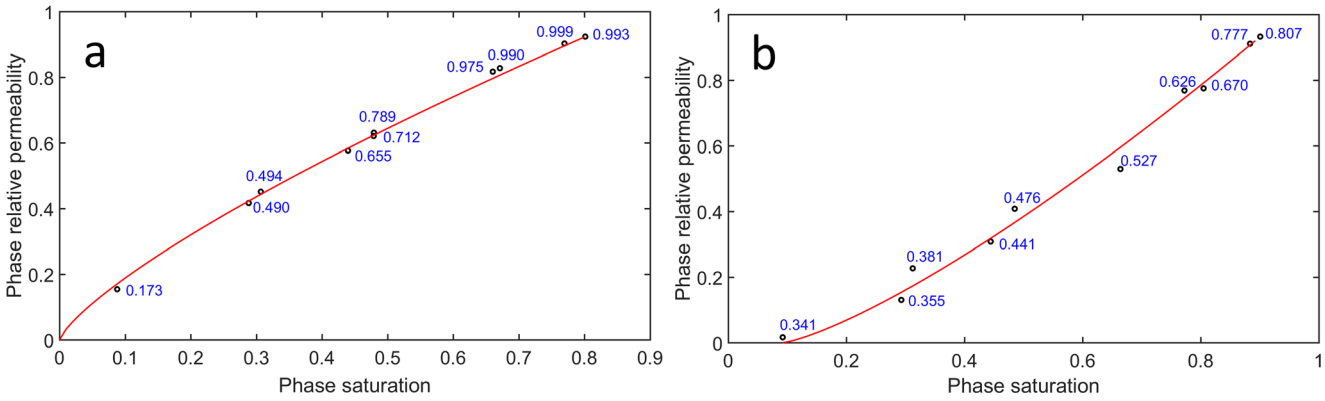

Fig. 9 Phase relative permeability plots with corresponding phase connectivity value (shown in blue). **a** High capillary number ~ 1. **b** Low capillary number $\sim 10^{-5}$. The red solid lines represent the fit using the Corey model with $\sim$ exponent value of **a** 0.76 and **b** 1.29. The residual saturation in **a** was set to 0 while computing the Corey exponent because that data point was not known

and provides a reasonable fit to the data presented in the literature. The presented approach is mathematically simple, which is advantageous for potential use in compositional simulation. The assumption of a quadratic response surface may not fit all relative permeability data, where higher-order polynomials may be needed. Nevertheless, the response surface approach developed here justifies the relative permeability functionality presented by Khorsandi et al. [22] for an exponent of 2.0. In addition, one of the main outcomes of using the developed EoS is being able to eliminate discontinuities resulting from using saturation-dependent relative permeability correlations in compositional simulators, which increases computational time and reduces accuracy. This would be especially useful to account for complex processes such as mass transfer and dynamic changes that often occur during transport of multiple phases in real porous media. A future research direction is to develop an improved functional form of relative permeability that honors physical limits and is more predictive than response surfaces.

Acknowledgments The authors thank ADNOC, Energi Simulation, OMV, Shell, and KOC for their partial financial support of this research through the EOR JIP at Penn State University, University Park, PA. The authors also thank Dr. Ryan T. Armstrong for providing the simulation data set used in this study. Drs. Johns and Karpyn hold the Energi Simulation Chair in Rock and Fluid Interactions at Penn State University. Dr. Russell Johns also holds the George E. Trimble Chair in Earth and Mineral Sciences.

Nomenclature A, B, C, Coefficients for planar representation of relative permeability for 2D extrapolation; α_i, Coefficients in the quadratic expression for relative permeability, $i = 0, 1, 2, 11, 22, 12$; $\beta_0, \beta_1, \beta_2$, Betti numbers 0, 1, and 2, respectively; E, Number of edges in a polyhedron; F, Faces in a polyhedron; I, Wettability index; k_{r_j}, Relative permeability of phase j; λ, Pore structure; Micro-CT, Micro-computed tomography; N_{ca}, Capillary number; P_{c}, Capillary pressure; PV, Pore volume; S_j, Saturation of phase j; V, Number of vertices in a polyhedron; $\hat{\chi}_j$, Normalized Euler connectivity; χ_j, Euler characteristic of phase j; $\chi_{\min}$, Euler characteristic representing the most connected state of a phase; $\chi_{\max}$, Euler characteristic representing the maximum disconnected state of a phase.

References

1. Parker, J.C.: Multiphase flow and transport in porous media. Rev. Geophys. **3**, 311–328 (1989)
2. Nadafpour, M., Rasaei, M.R.: Investigating drainage rate effects on fractal patterns and capillary fingering in a realistic glass micromodel. Teh. Vjesn. **21**, 1263–1271 (2014)
3. Bachu, S., Bennion, B.: Effects of in-situ conditions on relative permeability characteristics of CO2-brine systems. Environ. Geol. **54**, 1707–1722 (2008). https://doi.org/10.1007/s00254-007-0946-9
4. Gerhard, J.I., Kueper, B.H.: Relative permeability characteristics necessary for simulating DNAPL infiltration, redistribution, and immobilization in saturated porous media. Water Resour. Res. 39. https://doi.org/10.1029/2002WR001490 (2003)
5. Chang, L.C., Chen, H.H., Shan, H.Y., Tsai, J.P.: Effect of connectivity and wettability on the relative permeability of NAPLs. Environ. Geol. **56**, 1437–1447 (2009). https://doi.org/10.1007/s00254-008-1238-8
6. Lamanna, J.M., Bothe, J.V., Zhang, F.Y., Mench, M.M.: Measurement of capillary pressure in fuel cell diffusion media, micro-porous layers, catalyst layers, and interfaces. J. Power Sources. **271**, 180–186 (2014). https://doi.org/10.1016/j.jpowsour.2014.07.163
7. Akhgar, A., Khalili, B., Moa, B., Rahnama, M., Djilali, N.: Lattice-Boltzmann simulation of multi-phase phenomena related to fuel cells. AIP Conf. Proc. 1863. https://doi.org/10.1063/1.4992192 (2017)
8. Haines, W.B.: Studies in the physical properties of soil. Physics (College. Park. Md). 20 (1930)
9. Berg, S., Ott, H., Klapp, S.A., Schwing, A., Neiteler, R., Brussee, N., Makurat, A., Leu, L., Enzmann, F., Schwarz, J.-O., Kersten, M., Irvine, S., Stampanoni, M.: Real-time 3D imaging of Haines jumps in porous media flow. Proc. Natl. Acad. Sci. USA. 110. https://doi.org/10.1073/pnas.1221373110 (2013)
10. Roof, J.G.: Snap-off of oil droplets in water-wet pores. Soc. Pet. Eng. J. **10**, 85–90 (1970). https://doi.org/10.2118/2504-PA
11. Singh, K., Menke, H., Andrew, M., Lin, Q., Rau, C., Blunt, M.J., Bijeljic, B.: Dynamics of snap-off and pore-filling events during two-phase fluid flow in permeable media. Sci. Rep. **7**, 5192 (2017). https://doi.org/10.1038/s41598-017-05204-4
12. Mohanty, K.K., Davis, H.T., Scriven, L.E.: Physics of oil entrapment in water-wet rock. SPE Reserv. Eng. 2. https://doi.org/10.2118/9406-PA (1987)
13. Sahimi, M., Imdakm, A.O.: The effect of morphological disorder on hydrodynamic dispersion in flow through porous media. J. Phys. A. Math. Gen. **21**, 3833–3870 (1988). https://doi.org/10.1088/0305-4470/21/19/019
14. Al-Khulaifi, Y., Lin, Q., Blunt, M.J., Bijeljic, B.: Reaction rates in chemically heterogeneous rock: coupled impact of structure and flow properties studied by X-ray microtomography. Environ. Sci. Technol. **51**, 4108–4116 (2017). https://doi.org/10.1021/acs.est.6b06224
15. Menke, H.P., Bijeljic, B., Blunt, M.J.: Dynamic reservoir-condition microtomography of reactive transport in complex carbonates: effect of initial pore structure and initial brine pH. Geochim. Cosmochim. Acta. **204**, 267–285 (2017). https://doi.org/10.1016/j.gca.2017.01.053
16. Zhang, P., Austad, T.: Wettability and oil recovery from carbonates: effects of temperature and potential determining ions, vol. 279, pp. 179–187. https://doi.org/10.1016/j.colsurfa.2006.01.009 (2006)
17. Purswani, P., Tawfik, M.S., Karpyn, Z.: Factors and mechanisms governing wettability alteration by chemically tuned waterflooding: a review. Energy & Fuels. https://doi.org/10.1021/acs.energyfuels.7b01067 (2017)
18. Purswani, P., Karpyn, Z.T.: Laboratory investigation of chemical mechanisms driving oil recovery from oil-wet carbonate rocks. Fuel **235**, 406–415 (2019). https://doi.org/10.1016/j.fuel.2018.07.078
19. Khorsandi, S., Li, L., Johns, R.T.: A new way of compositional simulation without phase labeling. In: Society of Petroleum Engineers. Tulsa, Oklahoma, USA (2018)
20. Land, C.S.: Calculation of imbibition relative permeability for two- and three-phase flow from rock properties. Soc. Pet. Eng. J., pp. 149–156. https://doi.org/10.2118/1942-PA (1968)
21. Majid Hassanizadeh, S., Gray, W.G.: Toward an improved description of the physics of two-phase flow. Adv. Water Resour. **16**, 53–67 (1993). https://doi.org/10.1016/0309-1708(93)90029-F

22. Khorsandi, S., Li, L., Johns, R.T.: Equation of state for relative permeability, including hysteresis and wettability alteration. SPE J. **22**, 1915–1928 (2017). https://doi.org/10.2118/182655-PA
23. Berg, S., Rücker, M., Ott, H., Georgiadis, A., van der Linde, H., Enzmann, F., Kersten, M., Armstrong, R.T., de With, S., Becker, J., Wiegmann, A.: Connected pathway relative permeability from pore-scale imaging of imbibition. Adv. Water Resour. **90**, 24–35 (2016). https://doi.org/10.1016/j.advwatres.2016.01.010
24. Celauro, J.G., Torrealba, V.A., Karpyn, Z.T., Klise, K.A., Mckenna, S.A.: Pore-scale multiphase flow experiments in bead packs of variable wettability. Geofluids. **14**, 95–105 (2014). https://doi.org/10.1111/gfl.12045
25. Herring, A.L., Sheppard, A., Andersson, L., Wildenschild, D.: Impact of wettability alteration on 3D nonwetting phase trapping and transport. Int. J. Greenh. Gas Control. **46**, 175–186 (2016). https://doi.org/10.1016/j.ijggc.2015.12.026
26. Herring, A.L., Middleton, J., Walsh, R., Kingston, A., Sheppard, A.: Flow rate impacts on capillary pressure and interface curvature of connected and disconnected fluid phases during multiphase flow in sandstone. Adv. Water Resour. **107**, 460–469 (2017). https://doi.org/10.1016/j.advwatres.2017.05.011
27. Landry, C.J., Karpyn, Z.T., Ayala, O.: Relative permeability of homogenous-wet andmixed-wet porousmedia as determined by pore-scale lattice Boltzmann modeling. Water. **50**, 3672–3689 (2014). https://doi.org/10.1002/2013WR015148.Received
28. Karpyn, Z.T., Piri, M., Singh, G.: Experimental investigation of trapped oil clusters in a water-wet bead pack using X-ray microtomography. Water Resour. Res. **46**, 1–25 (2010). https://doi.org/10.1029/2008WR007539
29. Pak, T., Butler, I.B., Geiger, S., van Dijke, M.I.J., Sorbie, K.S.: Droplet fragmentation: 3D imaging of a previously unidentified pore-scale process during multiphase flow in porous media. Proc. Natl. Acad. Sci. **112**, 1947–1952 (2015). https://doi.org/10.1073/pnas.1420202112
30. Avraam, D.G., Payatakes, A.C.: Flow mechanisms, relative permeabilities, and coupling effects in steady-state two-phase flow through porous media. The case of strong wettability. Ind. Eng. Chem. Res. **38**, 778–786 (1999). https://doi.org/10.1021/ie980404o
31. Armstrong, R.T., McClure, J.E., Berrill, M.A., Rücker, M., Schlüter, S., Berg, S.: Beyond Darcy's law: The role of phase topology and ganglion dynamics for two-fluid flow. Phys. Rev. E. **94**, 1–10 (2016). https://doi.org/10.1103/PhysRevE.94.043113
32. Armstrong, R.T., Mcclure, J.E., Berill, M.A., Rücker, M., Schlüter, S., Berg, S.: Flow regimes during immiscible displacement. Int. Symp. Soc. Core Anal. **58**, 1–12 (2016)
33. Khishvand, M., Alizadeh, A.H., Piri, M.: In-situ characterization of wettability and pore-scale displacements during two- and three-phase flow in natural porous media. Adv. Water Resour. **97**, 279–298 (2016). https://doi.org/10.1016/j.advwatres.2016.10.009
34. Blunt, M.J.: Multiphase flow in permeable media: a pore-scale perspective. Cambridge University Press, Cambridge (2017)
35. Landry, C.J., Karpyn, Z.T., Piri, M.: Pore-scale analysis of trapped immiscible fluid structures and fluid interfacial areas in oil-wet and water-wet bead packs. Geofluids. **11**, 209–227 (2011). https://doi.org/10.1111/j.1468-8123.2011.00333.x
36. Avraam, D.G., Payatakes, A.C.: Flow regimes and relative permeabilities during steady-state two-phase flow in porous media. J. Fluid Mech. **293**, 207–236 (1995). https://doi.org/10.1017/S0022112095001698
37. Cleveland, C., Morris, C.: Dictionary of energy. Elsevier Science & Technology, Amsterdam (2014)
38. Sandler, S.I.: Chemical and engineering thermodynamics. Wiley, New Jersey (1989)
39. Osborne, G.A.: Differential and integral calculus: with examples and applications. D.C. Heath & Co. (1908)
40. Schlüter, S., Berg, S., Rücker, M., Armstrong, R.T., Vogel, H.J., Hilfer, R., Wildenschild, D.: Pore-scale displacement mechanisms as a source of hysteresis for two-phase flow in porous media. Water Resour. Res. **52**, 2194–2205 (2016). https://doi.org/10.1002/2015WR018254
41. Aydogan, D.B., Hyttinen, J.: Contour tree connectivity of binary images from algebraic graph theory. In: 20Th IEEE International Conference on Image Processing (ICIP), pp. 3054–3058. IEEE, Melbourne (2013)
42. Vogel, H.-J.: Topological characterization of porous media. Morphol. Condens. Matter, Ed. by K. Mecke, D. Stoyan, Lect. Notes Phys. 600, pp. 75–92. https://doi.org/10.1007/3-540-45782-83 (2002)
43. Hovadik, J.M., Larue, D.K.: Static characterizations of reservoirs: refining the concepts of connectivity and continuity. Pet. Geosci. **13**, 195–211 (2007). https://doi.org/10.1144/1354-079305-697
44. Allard, D.: Some Connectivity Characteristics of a Boolean Model. In: Geostatistics Troia '92. Quantitative Geology and Geostatistics, pp. 467-478. Springer, Dordrecht (1993)
45. Aydogan, D.B., Hyttinen, J.: Characterization of microstructures using contour tree connectivity for fluid flow analysis. J. R. Soc. Interface **11**, 20131042–20131042 (2014). https://doi.org/10.1098/rsif.2013.1042
46. Richeson, D.S.: Euler's Gem: the polyhedron formula and the birth of topology. Princeton University Press, Princeton (2008)
47. Herring, A.L., Harper, E.J., Andersson, L., Sheppard, A., Bay, B.K., Wildenschild, D.: Effect of fluid topology on residual nonwetting phase trapping: implications for geologic CO2 sequestration. Adv. Water Resour. **62**, 47–58 (2013). https://doi.org/10.1016/j.advwatres.2013.09.015
48. Delshad, M., Delshad, M., Pope, G.A., Lake, L.W.: Two- and three-phase relative permeabilities of micellar fluids. SPE Form. Eval. **2**, 327–337 (1987). https://doi.org/10.2118/13581-PA